Inner-shell photodetachment from Ru^-

I. Dumitriu,[1,*] R. C. Bilodeau,[1,2] T. W. Gorczyca,[1] C. W. Walter,[3] N. D. Gibson,[3] Z. D. Pešić,[1,2,†] D. Rolles,[1,2,‡] and N. Berrah[1]

[1]*Department of Physics, Western Michigan University, Kalamazoo, Michigan 49008, USA*

[2]*Advanced Light Source, Lawrence Berkeley National Laboratory, Berkeley, California 94720, USA*

[3]*Department of Physics and Astronomy, Denison University, Granville, Ohio 43023, USA*

(Received 25 July 2010; published 26 October 2010)

Inner-shell photodetachment from Ru^- was studied near and above the $4p$ excitation region, 29-to-91-eV photon energy range, using a merged ion-photon-beam technique. The absolute photodetachment cross sections of Ru^- ([Kr] $4d^7 5s^2$) leading to Ru^+, Ru^{2+}, and Ru^{3+} ion production were measured. In the near-threshold region, a Wigner s-wave law, including estimated postcollision interaction effects, locates the $4p_{3/2}$ detachment threshold between 40.10 and 40.27 eV. Additionally, the Ru^{2+} product spectrum provides evidence for simultaneous two-electron photodetachment (likely to the Ru^+ $4p^5 4d^6 5s^2$ state) located near 49 eV. Resonance effects are observed due to interference between transitions of the $4p$ electrons to the quasibound $4p^5 4d^8 5s^2$ states and the $4d \rightarrow \varepsilon f$ continuum. Despite the large number of possible terms resulting from the Ru^- $4d$ open shell, the cross section obtained from a 51-state LS-coupled R-matrix calculation agrees qualitatively well with the experimental data.

DOI: 10.1103/PhysRevA.82.043434 PACS number(s): 32.80.Gc, 32.80.Aa, 32.70.Fw, 32.30.Rj

I. INTRODUCTION

The demand for materials with special qualities has focused attention on the properties of the transition elements containing partially filled d orbitals. Transition metals are of interest because of their catalytic properties and the participation of d-orbital electrons in bonding properties. The transition metals and their compounds are of extreme practical importance in metallurgy, utilization of marine resources, cosmochemistry, and geology [1]. In addition, understanding the magnetic properties of transition-metal thin films is crucial for modern data-storage technology [2]. The interaction of transition-metal atoms and ions with electromagnetic radiation generates very complex spectra due to the coupling of d electrons with core holes and the underlying continua [3]. The angular momentum coupling leads to a large number of possible terms from the open d shell; thus, for an accurate description of the photoionization process, strong correlations between these terms as well as relativistic effects have to be taken into account [2–4]. The d orbital retains, to a high degree, the same characteristics in solids [3,4], so the atomic and ionic data could be very useful for contributing information toward understanding intra- and interatomic effects.

Throughout the universe, transition metals are abundant, and ruthenium is the most abundant of the platinum-group metals (i.e., Ru, Rh, Pd, Os, Ir, and Pt) in meteoritic matter [5]. The ruthenium atom is of interest for providing an efficient conversion of solar energy into chemical energy by photoinduced electron transfer [6]. Due to the experimental difficulties of producing a usable atomic beam, mainly the high temperature required to vaporize the metal (boiling point 4150°C [7]), there have been few experimental and theoretical studies of free ruthenium atoms [1,8–10] compared to the situation for solids [4,11–14]. Only one valence-shell photodetachment study exists for the ruthenium negative ion [15], in which laser photodetachment spectroscopy was used to measure the binding energies of the ground-state Ru^- ([Kr] $4d^7 5s^2\, {}^4F_{9/2}$) [1.046 38(25) eV, the electron affinity of Ru] and the first excited fine-structure level $^4F_{7/2}$ [0.8653(10) eV] together with calculations for the $^4F_{5/2}$ (0.795 eV) and $^4F_{3/2}$ (0.725 eV) levels.

It is well known that the photoionization cross sections of d-photoelectron bands of gas-phase molecules are highly structured. A massive variation in the cross section, the so-called "giant resonance," has been observed, for example, at about 55 eV in the d-band photoelectron spectrum of $Ru(\eta\text{-}C_5H_5)_2$ [4], as well as seen or predicted in other transition metals [2,3,16]. It is therefore of interest to determine if a similar giant resonance is also present in the photodetachment cross section of the Ru^- atomic negative ion.

In this work, the photodetachment cross section for Ru^- was obtained by measuring the Ru^+, Ru^{2+}, and Ru^{3+} ion production over the photon energy range 29–91 eV. The absolute cross sections for the production of Ru^+, Ru^{2+}, and Ru^{3+} were measured at three photon energies (see Sec. III A). The experimental results are compared to a 51-state LS-coupled R-matrix calculation (see Sec. III B), which shows good qualitative agreement, although some structures in the experimental results are not reproduced. Evidence of a giant resonance is observed in both experiment and theory, as seen as a broad interference structure between transitions of the $4p$ electrons to the quasibound $4p^5 4d^8 5s^2$ states and the $4d \rightarrow \varepsilon f$ continuum.

II. EXPERIMENTAL METHOD

The experiment was performed at the Advanced Light Source (ALS) using the High-Resolution Atomic, Molecular and Optical Physics (HRAMO) undulator beamline 10.0.1 with the fixed ion-photon beamline (IPB) end station [17]. The

*Present address: Department of Physics, Gustavus Adolphus College, St. Peter, MN 56082.

†Present address: Diamond Light Source, Harwell Science and Innovation Campus Didcot, OX11 0DE, United Kingdom.

‡Present address: Max Planck Advanced Study Group, Center for Free Electron Laser.

IPB is based on a counterpropagating merged-beam technique for photoion spectroscopy in order to increase the interaction volume between photons and the dilute ion beam.

The experimental technique has been described previously [18–22]. A 7.54-keV negative-ion beam of Ru^- was produced using a cesium sputter source (SNICS II, from NEC) [23], with an ion current of about 40 nA obtained in the interaction region after shaping and spatial trimming. The magnetically mass-selected negative-ion beam with a diameter of ~5 mm overlapped the counterpropagating photon beam with a spatial width of ~1.2 mm over a distance of about 1.5 m. Inner-shell photodetachment and subsequent Auger decay produce positive ions that were deflected by the demerger magnet and counted as a function of photon energy with an electron-multiplier-based detection system.

The photon-ion interaction region was defined by a ~30-cm-long stainless-steel cylinder, held at +0.55 kV in order to kinetic-energy tag the Ru^- ions. Negative ions entering in the interaction region were thus accelerated to 8.09 keV, and the positively charged ions Ru^+ (or Ru^{2+}) resulting from the photodetachment process exited the interaction region experiencing a second kinetic energy boost of +0.55 keV (or +1.10 keV), leaving with 8.64 keV (or 9.19 keV) kinetic energy. The Ru^+ and Ru^{2+} ions formed outside of the interaction region, having a lower kinetic energy of 7.54 keV, could then be easily rejected by the demerger magnet and spherical electrostatic deflector located before the detector. The ion-photon beam overlap was optimized by using two rotating-wire beam profile monitors near the entrance and exit of the interaction region. In addition, three translating-slit scanners located near the entrance, middle, and exit of the interaction region were used to obtain two-dimensional (2D) profiles of the photon and ion beam. In this way the interaction volume was well defined, which allowed for absolute cross-section measurements (see Sec. III A).

The ground states of Ru, Ru^+, Ru^{2+}, Ru^{3+}, and Ru^{4+}, relative to the Ru^- ground state are, respectively, 1.046 38(25) [15], 8.4069(3) [9], 25.167(10) [24], 58.8(26) [25], and 108(5) eV [25] [uncertainties are quoted to 1 standard deviation (SD) throughout]. Ru^{4+} and higher charged-state products are therefore not energetically possible to produce with the photon energies used in the present experiment. All three energetically allowed ionic products were measured. Note that only charged products can be detected with the present apparatus and neutral Ru, although very likely produced, could not be detected.

A significant background signal was produced by collisions between negative ions and residual vacuum gas (~4×10^{-10} torr) or apertures in the beamline. The photon beam was chopped at 6 Hz in order to continuously monitor and subtract the background signal. The resulting photodetachment signal was normalized to the incident photon flux and the negative-ion current. The incident photon flux was recorded by an absolutely calibrated silicon x-ray photodiode [26] and the ion current was monitored with a Faraday cup placed after the demerging magnet. The effects of any variations over time of the experimental parameters (ion-photon-beam overlap, negative-ion current, incident photon flux, vacuum gas pressure) could therefore be monitored and corrected for (see Sec. III A for details on the effects of these experimental parameters on the cross section). Several sweeps over the photon energy of interest were recorded and summed in order to improve the signal-to-noise ratio.

The photon energy was scanned by rotating the spherical-grating of the monochromator and translating the exit slit of the monochromator while simultaneously adjusting the undulator gap to maximize the photon-beam intensity. The Ru^--beam energy in the interaction region was determined to be 8.09(20) keV, which gives sufficient ion velocity to produce a small Doppler shift, between 12 and 37 meV for photon energies between 29 and 91 eV. The monochromator photon energy was calibrated using accurately known absorption lines of Ar [27], Ne [28], and He [29]. The resulting uncertainty in the calibration was between 10 meV (at 30 eV) and 180 meV (at 90 eV). Corrections for the photon energy calibration and Doppler shift have been applied to all the spectra reported here.

III. RESULTS AND DISCUSSION

A. Absolute cross sections

The absolute cross section for production of a photodetachment product is given by the formula $\sigma = qvR/I\Phi F$ [17], where q is the charge of the target ion, R is the signal rate, Φ is the photon flux, I is the target-ion current, v is the velocity of negative ions, and F is the form factor. The signal rate is $R = R_0/(\Omega_{\mathrm{det}}\Omega_{\mathrm{electr}})$, where R_0 is the measured count rate, Ω_{det} is the detector efficiency, and Ω_{electr} is the pulse detection efficiency of the electronics. In the present experiment the detector efficiency Ω_{det} was estimated to be 100(7)% [30] and Ω_{electr} was 99(1)%. (Note that we include the possibility of $\Omega_{\mathrm{det}} > 100\%$ to account for possible double-counting events arising from electronic ringing and other effects.)

The 2D form factors $F_z = \int i_x \Phi_x dx \int i_y \Phi_y dy$ were calculated based on ion i and photon Φ beam profiles measured at three positions by slit scanners, where x and y are orthogonal directions in the plane normal to the ion- and photon-beam propagation direction. The total form factor F, a measure of the photon-ion beam overlap quality, is then obtained by integrating the quadratic interpolation of 2D form factors (measured at three positions) over the biased interaction region length of 28.3(14) cm, determined from electrostatic simulations using SIMION 7.00 [31], and the ion kinetic-energy acceptance of the positive-ion detection system. The total (1 SD) systematic instrumental error in the absolute cross section was ±20%.

The measured absolute cross sections for photoexcitation of Ru^- leading to Ru^+, $\sigma(Ru^+)$, are listed in Table I. The cross sections for Ru^{2+} and Ru^{3+} production were obtained by multiplying these by the ratio of the cross sections, $\sigma(Ru^{2+})/\sigma(Ru^+)$ and $\sigma(Ru^{3+})/\sigma(Ru^+)$, also listed in Table I. As in previous experiments [18–21], these ratios were determined by recording the signal rates for each photoionization product in rapid succession (typically 1–4 min per product per energy point). The measurements were repeated several times to verify that no significant fluctuations in the overlap, ion current, or other such effects affected the results.

B. Broad-range spectra—giant resonance region

The total photodetachment cross sections for Ru^+ from Ru^- were measured in the 29-to-91-eV photon energy range,

TABLE I. Absolute photodetachment cross sections σ for the production of Ru^+, Ru^{2+}, and Ru^{3+} from Ru^-, obtained from the measured $\sigma(Ru^+)$ cross section and the ratios, $\sigma(Ru^{2+})/\sigma(Ru^+)$ and $\sigma(Ru^{3+})/\sigma(Ru^+)$, which are also reported. All values are reported to 1 SD.

	Cross section (Mb)			Measured ratio (%)	
Photon energy (eV)	Ru^+	Ru^{2+}	Ru^{3+}	$\sigma(Ru^{2+})/\sigma(Ru^+)$	$\sigma(Ru^{3+})/\sigma(Ru^+)$
48.663(15)	9.5(19)	1.03(22)	0.0044(14)[a]	10.8(8)	0.046(11)
69.26(5)	5.3(11)	2.1(4)	0.030(7)	39.7(28)	0.58(7)
89.35(18)	1.35(29)	0.80(18)	0.065(15)	59(4)	4.8(4)

[a]Note: it is impossible to produce Ru^{3+} at photon energies below 58.8 eV, and this small cross section is therefore due to some contamination (see text).

as shown in Fig. 1. The reported spectra were normalized to the absolute cross-section measurements, represented as large circles with 1-SD error bars. The relevant states in the Ru atom and ions are presented in Fig. 2. Below the $4p$ threshold at ~40 eV (binding energies of 43.2 eV for the $4p_{3/2}$ and 46.3 eV for the $4p_{1/2}$, relative to the Fermi surface, have been measured in Ru metal samples [32]), a significant photodetachment cross section is observed. While some of this Ru^+ signal may be produced by simultaneous (direct) double photodetachment of $5s$ and/or $4d$ electrons, we find from multiconfiguration Hartee-Fock (MCHF) calculations (see later in this article) that there are several excited triplet states of Ru above the $4d^7\,{}^4F$ ground state of Ru^+. Photodetachment into one of these states would quickly autoionize, explaining the strong signal below the $4p$ threshold. Below 40 eV there is a strong dip, followed by a sharp increase in the cross section near the $4p_{3/2}$ threshold. This is followed by a large structure with a maximum cross section of more than 10 Mb at about 46.5 eV and a slow, broad decay of the underlying continua.

Recently we investigated the photodetachment cross section of Fe^-, where three large, well-separated shape resonances were observed in the 48-to-72-eV photon energy range [19].

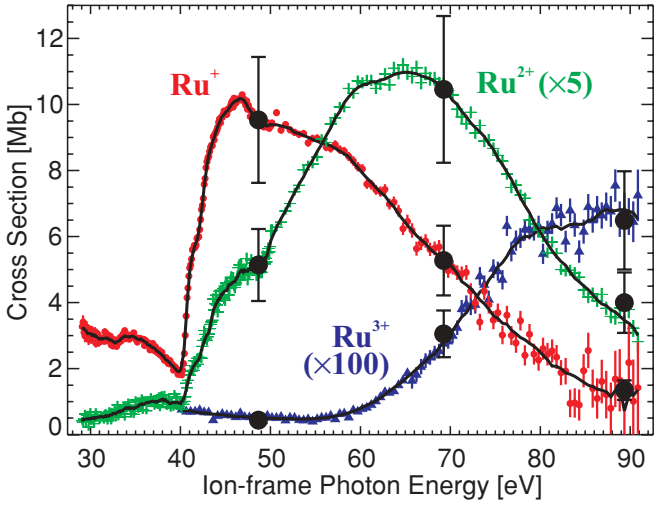

FIG. 1. (Color online) High-resolution (100 meV) measured photodetachment cross section for Ru^+, Ru^{2+}, and Ru^{3+} from Ru^-. The cross-section scale was established by making absolute measurements (denoted by solid circles) at the three energies shown. Solid curves are the data smoothed over several data points and are included to help guide the eye. For clarity of presentation, the cross section has been multiplied by a factor of 5 for Ru^{2+} and 100 for Ru^{3+}.

Despite the similar electronic configuration of Fe^- ([Ar] $3d^7 4s^2\,{}^4F$) and Ru^- ([Kr] $4d^7 5s^2\,{}^4F$), the behavior of their photodetachment cross sections in the $np \rightarrow nd$ excitation region ($n = 3$ for Fe^-, and $n = 4$ for Ru^-) is strikingly different.

Shape resonances are situated just above their parent atomic state. In this case the one-electron potential produced by the short-range attraction and the centrifugal repulsion forms a barrier large enough to trap the electron behind it. The primary decay mechanism is tunneling through the barrier, and thus the width and strength of the resonances are influenced by the particular form of the potential. This resonance behavior has been reported for other inner-shell photodetachment studies, such as in Li^- [33–36], B^- [22,37,38], C^- [39–41], and Fe^- [19]. As a consequence of their decay mechanism, the resonances are broad structures in the photodetachment cross section and since they are often located very close to a threshold, the corresponding Wigner threshold behavior is severely altered by their presence, as pointed out by

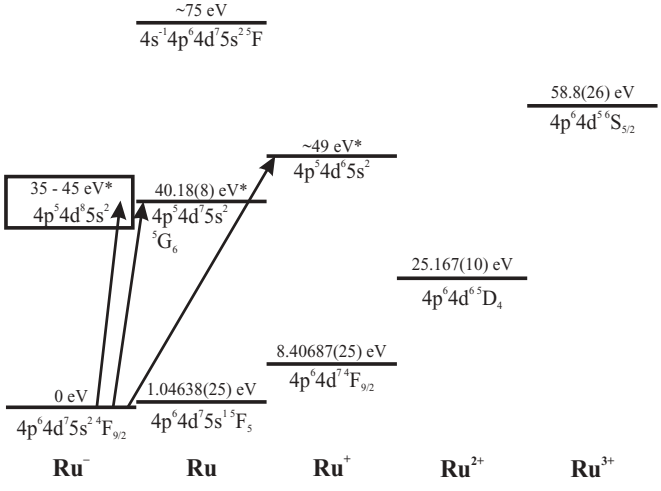

FIG. 2. Energy-level diagram (to scale) showing ground [9,24,25] and some relevant core excited states of Ru^-, Ru, Ru^+, Ru^{2+}, and Ru^{3+}, relative to the ground state of Ru^- [15] (the $4s$ detachment threshold is estimated from [47]). Included is a preliminary assignment of $4p^5 4d^6 5s^2$ for the core-excited state responsible for the two-electron detachment threshold discussed in Sec. III C. For clarity of presentation, fine-structure states are not shown. An asterisk (*) indicates that the level energy is obtained from this work. The very broad "giant" Ru^- $4p^5 4d^8 5s^2$ resonant excitations observed in this work are indicated as a range of energies (depicted by a box) around the $4p$ detachment threshold based on the measured and calculated theoretical spectra. The arrows indicate channels leading to the main structures described herein.

Peterson *et al.* [42,43]. Such shape resonances describe the Fe^- photodetachment spectrum very well, as can be seen by the excellent fit of a sum of three modified shape resonance profiles to the experimental data [19]. However, these profiles poorly describe the Ru^- photodetachment cross section, indicating that the nature of these structures is likely different.

The Ru^- spectrum resembles much more closely that which is expected from Cr^-([Ar] $3d^5 4s^2\ ^6S_{5/2}$), where a giant resonance is predicted (see *ab initio* calculations of Ivanov *et al.* [16], which appear to be in reasonable agreement with unpublished experiments reported by Kjeldsen [44]). This resonance is similar to giant autoionizing resonances in the $3p$ photoionization spectra of the neutral $3d$ transition metals and their positive ions [2,3]. Unlike Fe^-, the Cr^- spectrum appears to be highly modified by interchannel interaction [16]. There, the $3p \rightarrow 3d$ resonance is expected to have a large effect on the $3d \rightarrow \varepsilon f$ channel, appearing as a pronounced Fano-profile structure in that partial wave. It appears that such interchannel coupling is also more prominent in Ru^- than the lighter Fe^- system, and may explain some of the differences between these two systems. It is also interesting to note in this regard that the ground state configurations of neutral Cr and Ru both have a single s electron in the valence shell as opposed to Fe, in which the outer s shell is filled. As in Cr^-, the dip and enhancement around the $4p$ threshold observed in Ru^+ production appears to be due to transitions of the $4p$ electrons to a quasibound state $4p^5 4d^8 5s^2$ in the $4d \rightarrow \varepsilon f$ continuum and is supported by our R-matrix calculations discussed below.

In order to study the photodetachment of Ru^- theoretically, we use the R-matrix method [45] as follows. First, a Hartree-Fock calculation was performed for the configuration-averaged $4p^6 4d^6 5s^2$ state to generate a basis set of $1s$, $2s$, $2p$, $3s$, $3p$, $3d$, $4s$, $4p$, $4d$, and $5s$ orbitals. Then a 51-state LS-coupled R-matrix calculation was performed including all 20 even-parity target states of Ru that could be coupled from the $4p^6 4d^6 5s^2$,$4p^6 4d^7 5s$, and $4p^6 4d^8$ configurations and all 31 odd-parity target states that could be coupled from the $4p^5 4d^7 5s^2$, $4p^5 4d^8 5s$, and $4p^5 4d^9$ configurations. Since the ground state of Ru^- is of ^4F symmetry, dipole selection rules dictate that the ^4G, ^4F, and ^4D final symmetries can be populated via photodetachment.

We first present the total photodetachment cross section, summed over all three final symmetries and all energetically available channels (Th_{tot}) in Fig. 3, which shows strong distortion arising from $4p \rightarrow 4d$ excitations. Most of the cross section is due to the $4d$ and $5s$ photodetachment to the lowest 20 even-parity states. MCHF calculations locate the majority of these states below the Ru^+ ground state, which therefore cannot autoionize to ionic products, with only five triplet states above the Ru^+ ground state (in particular, in order of energy, the $4d^6[^3F_2]5s^2\ ^3F$, $4d^6[^3P_2]5s^2\ ^3P$, $4d^7[^2D_1]5s\ ^3D$, $4d^8\ ^3F$, and $4d^8\ ^3P$ states). The large discrepancy in the magnitude of the calculated total cross section and the measured cross section is therefore due to the fact that neutral Ru channel is not observed. Nonetheless, the shape of the total calculated cross section is very similar to the measured Ru^+ cross section, although shifted by about 2 eV to lower energies. This includes details such as a kink observed on the rising slope of the cross section, just above 40 eV in the experiment. Also well reproduced is the dip seen just below the $4p$ threshold and the maximum just above, arising from $4p \rightarrow 4d$ interference with the εf continuum.

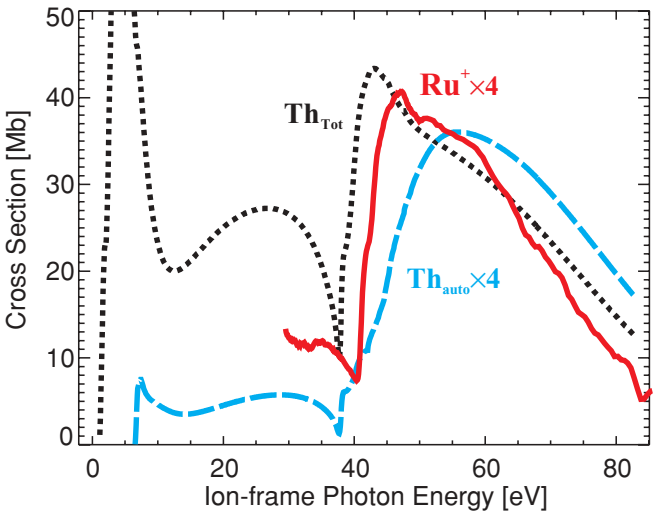

FIG. 3. (Color online) Total photodetachment cross section from 51-state LS-coupled R-matrix calculation (Th_{tot}). The partial cross section for 36 autoionizing states is also shown (Th_{auto}, magnified by a factor of 4 for clarity of presentation). The measured Ru^+ spectrum is plotted for comparison (the curve is five-point smoothed and magnified by a factor of 4).

To attempt to better understand the observed Ru^+ spectrum, we calculate the sum of the autoionizing states, that is, those we expect to lie above the Ru^+ ground state. These states include the five aforementioned triplet states and 31 $4p$ core-hole states. The partial cross section to these highest 36 target states (Th_{auto}) is also shown in Fig. 3. The strength and shape of the $4p$ continua are reasonably well reproduced (with a shift to higher energies) and part of the below-threshold signal is explained; however, almost all of the strong $4p \rightarrow 4d$ resonance strength is lost. One possibility is that the MCHF calculation is underestimating the energies of the excited Ru states. Indeed, including some additional lower-lying states restores the resonance structure (see Fig. 4), although the calculated cross section is approximately twice as large as the experiment. An alternate likely explanation is that the calculated oscillator strength is confined to low-lying Ru states by the limited basis used and should actually be redistributed to various other higher-lying states. We note, for example, that if configuration interaction is allowed with higher states for the Ru^- ground state, we obtain roughly 16% mixing of the $4d^7 5s^2$ and $4d^7 5p^2$ configurations. This makes photodetachment into Ru $4d^6 5p^2$ states possible, for example, which are autoionizing and could easily account for the missing oscillator strength in Th_{auto}. Therefore, overall, the calculations reproduce all the major features observed quite well; however, it would appear that there are additional autodetaching Ru excited states which carry some of the $4p \rightarrow 4d$ excitation cross section to Ru^+ that are missed in the sum.

C. Ru^{2+} and Ru^{3+} production

Further differences between Fe^- and Ru^- can be observed by comparing the doubly charged product (see Fig. 1). While the resonance region is essentially identical in Fe^+ and Fe^{2+},

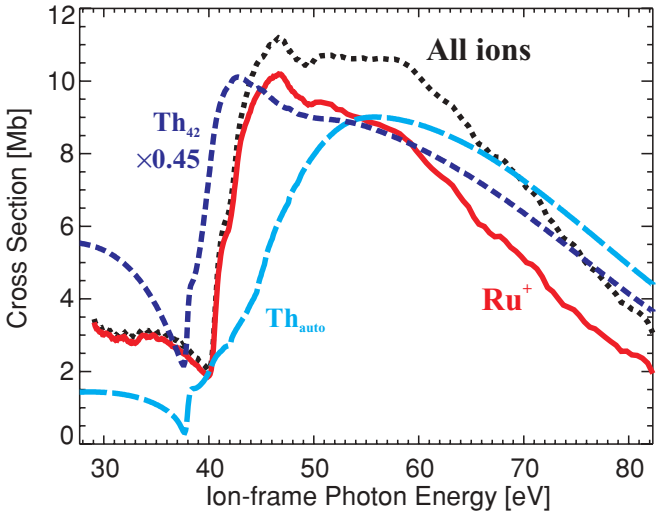

FIG. 4. (Color online) Comparison of theory with experiment. Experimental curves are for Ru^+ and the sum of all detected ionic products, as labeled (curves are smoothed over five data points to reduce statistical scatter). The sum of the 36 predicted autodetaching states (Th_{auto}) is observed to be lacking the resonant enhancement see in the experiment. Including the 42 highest-lying states (Th_{42}) recovers the structure, but has a cross section approximately a factor of 2 too large.

Ru^{2+} shows a remarkably modified spectrum. There are two main differences between the Ru^{2+} and the Ru^+ spectra. First, the dip below, and the maximum above, the $4p$ threshold are suppressed in the Ru^{2+} spectrum. This is because the $4p \rightarrow 4d$ resonance structure is not observed in the $4p \rightarrow \varepsilon d$, continuum, in striking contrast to Fe^-. Therefore, these excitations are only seen as an interference with the even states, all of which are well below the Ru^{2+} ground state. In order to compare with the calculations, Fig. 5 shows the measured

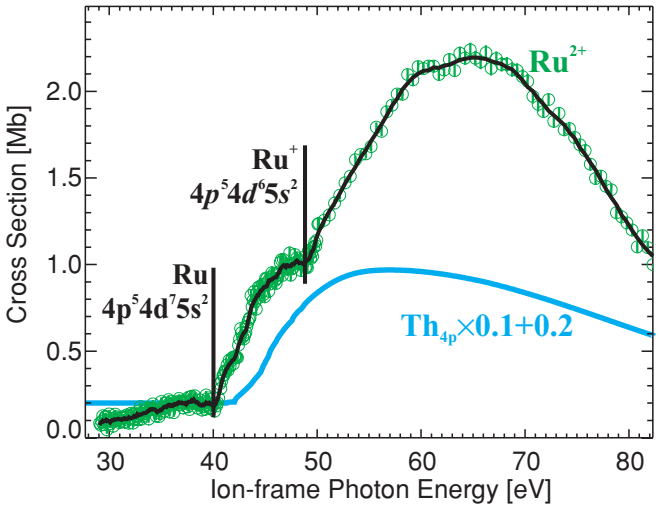

FIG. 5. (Color online) Comparison of the measured Ru^{2+} spectrum with the calculated cross section including only $4p$ core-hole states (Th_{4p}). The theory curve has been reduced by a factor of 10, to account for the low branching decay leading to Ru^{2+} and shifted up by 0.2 Mb, to estimate the small photodetachment background observed below the $4p$ threshold.

Ru^{2+} spectrum with the calculated cross section leading to states with a $4p$ hole only. The theory curve has been reduced by a factor of 10, reflecting that most of the cross section leads to single ionization, and shifted up by 0.2 Mb to estimate the observed below-threshold signal. There is a small shift, and perhaps stretch, in the photon energy scale (as also seen with the preceding comparison to Ru^+), but the calculations offer a reasonable description of the near-threshold region until ~49 eV, where the second difference with Ru^+ is seen. There appears to be an onset of a strong channel present in Ru^{2+} at ~49 eV that is absent in Ru^+. This energy corresponds roughly to where the excited state of Ru^+ $4p^5 4d^6 5s^2$ might be expected. This would represent a simultaneous (direct) two-electron detachment process from Ru^-, that is, where a $4d$ electron is knocked off in the $4p$ photodetachment process. While the energy of this state is not known, it can be roughly estimated assuming similar $4d$ binding energy as in the ground-state neutral atom [46], that is, ~8.5 eV above the $4p$ threshold. Due to the efficiency of Auger decay processes, this state will result almost exclusively in Ru^{2+} production, with no Ru^+ production, thus explaining why it is seen only in the Ru^{2+} channel. To further support this interpretation, we note that the same two-electron photodetachment process (except involving the $3p$ and $3d$ electrons) was observed in Fe^- at 57.0 eV (6.5 eV above the $3p$ threshold), although in Ru^- this channel appears to be relatively stronger.

Finally, as noted previously, it is possible to form Ru^{3+} at the higher photon energies explored here. However, only a very small cross section was observed [measured to be 65(15) kb at 89 eV; see Table I]. This is largely because the ground state of Ru^{3+} [at 58.8(26) eV relative to the ground state of the negative ion; see Fig. 2] is above the $4p$ detachment threshold, and therefore Auger decay channels from this core-hole are not available. Note, however, that a very small, slowly varying signal (<5 kb) is observed even below 58.8 eV. It is energetically impossible to form Ru^{3+} at these photon energies, and this signal must therefore arise from some contamination. The most likely source is from higher-order light in the photon beam. This type of contamination has been observed previously (see, e.g., [18]), especially with very low signal rate products with cross sections that increase substantially with photon energies, as is the case here. Finally, we note that the $4s$ threshold should open around 75 eV (estimated from measurements in solid samples [47]) and therefore could contribute to four-electron detachment at these higher energies but cannot explain the turn-on in the signal observed around 56 eV. The location of this apparent threshold is suggestive of a simultaneous (or "direct") four-electron detachment process to the ground state of Ru^{3+}. Such a process would be described by a Wannier threshold law [48], the cross section for which, for four-electron detachment, would follow a power law with an exponent of 3. The magnitude of the cross section, however, would be surprisingly large for such a four-electron process, as <1 kb at ~20 eV above threshold is expected based on measurements in other systems [49]. It may then be more likely that the process is a three-electron photodetachment into an autodetaching Ru^{2+} state. This would be described by a power law exponent of 2. Unfortunately, due to the underlying, possibly nonlinear, background observed in this channel and the extreme sensitivity of the threshold

position and power law to variations in the background signal, conclusive fits could not be made to the data. Fits nonetheless suggest a threshold position of between 49 and 60 eV, and a power law exponent between 2 and 3, which is consistent with the preceding interpretations.

D. 4*p* photodetachment threshold region

Negative ions are bound in a short-range potential ($\sim 1/r^4$) and this leads to a near-threshold photodetachment cross-section behavior significantly different than the behavior of atoms and positive ions, which are bound in the long-range Coulomb potential ($\sim 1/r$). In the case of negative ions, the near-threshold cross section follows the Wigner law [50]:

$$\sigma = \sigma_0 (h\nu - \varepsilon_t)^{l+1/2}, \tag{1}$$

where σ_0 is the amplitude, $h\nu$ is the photon energy, ε_t is the threshold energy, and $l = |l_0 \pm 1|$ is the photoelectron angular momentum, with l_0 the angular momentum of the bound electron being detached.

In the present experiment, if a $4p$ electron ($l_0 = 1$) is detached from Ru^-, the photoelectron angular momentum ($l = |l_0 \pm 1|$) can be 0 or 2, that is, an s or d wave. It has been seen in previous outer-shell photodetachment experiments [51] that the d wave is greatly suppressed by the centrifugal barrier and the photodetachment cross section near threshold is described by the Wigner s-wave law. Figure 6 shows the near-threshold photodetachment cross section of Ru^- obtained by measuring the positive-ion production for Ru^+ and Ru^{2+}

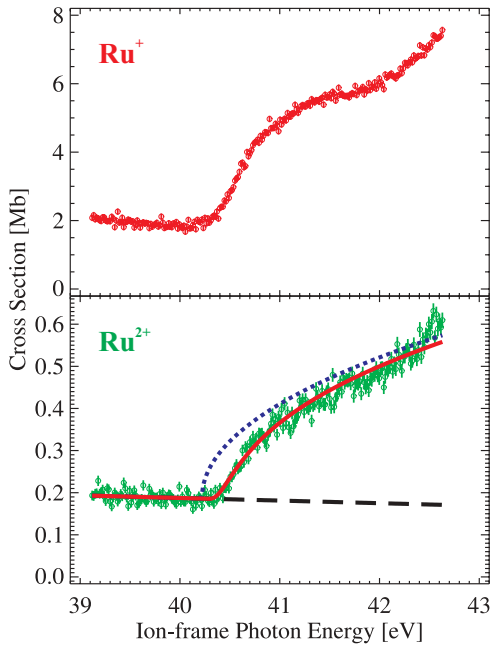

FIG. 6. (Color online) High-resolution (30 meV) photodetachment cross section of Ru^- leading to Ru^+ and Ru^{2+} measured near the $4p$ threshold. The open circles are the experimental data. The solid curve is a Wigner s profile fit to the data with inclusion of PCI effects, assuming an Auger width of 40 meV. The dotted curve is a Wigner s-wave law obtained from the fit with the PCI effects removed. The dashed curve represents the linear background included in the fit.

in the photon energy range from 39 to 42.5 eV with a photon energy resolution of 30 meV.

The Wigner threshold law has been verified in countless valence-shell detachment experiments [51]. Recent work in He^- ($1s$), S^- ($2p$) [20], Pt^- ($4f$) [18], and Fe^- ($3p$) [19] has shown that the Wigner p-, s-, and d-wave detachment threshold laws are also valid in inner-shell detachment, despite possibly significant postcollision interaction (PCI) effects. At photon energies very near a photodetachment threshold, the photoelectron has little kinetic energy and recedes from the atomic core very slowly. It is then possible for the fast electron released from the subsequent Auger decay to overtake the photoelectron before it has moved very far from the atomic core. Once overtaken, the photoelectron can get trapped in the exposed Coulomb potential of the residual ionic core. This results in a neutral atom instead of a positive ion product and hence the suppression of the detected positive ion production near the photodetachment threshold (unless the electron is recaptured in an autodetaching state [39]). The result is mainly an apparent shift of the threshold position to higher energies, dependent on the Auger decay lifetime, with some "smearing" of the threshold that is especially apparent in the sharp (infinite slope) turn on of s-wave threshold laws (see [20]). This signal suppression effect can be accurately accounted for by using a semiclassical reduction factor (see, for example, Ref. [36]).

The Ru^+ near-threshold data suffer from significant distortion due to the strong variations in the underlying photodetachment continua due to the $4d$ resonant interference discussed previously, which significantly obscures the threshold behavior. We note that studies in Pt^- had similar difficulties for the Pt^+ product [18]. However, in the case of Ru^{2+}, the continuum is near constant and a Wigner s-wave law fits the threshold region very well except very near to the threshold, where PCI effects become important, as discussed earlier. Unfortunately, the Auger decay lifetime for Ru $4p^5 4d^7 5s^2$ state is not known, and the decay width of the state couples very sensitively to the position of the threshold in the fit. The solid curve in Fig. 6 is a Wigner law (with the inclusion of the PCI effects assuming an Auger width of 40 meV) fit to the Ru^{2+} data from 39.5 to 41.5 eV, yielding a $4p_{3/2}$ threshold position of 40.2 eV. The dashed curve is the Wigner law obtained from the fit with the PCI effects removed and highlights the significant ($\sim$200 meV) apparent shift in the threshold position due to the PCI photoelectron recapture effect. While the solid curve is an excellent fit to the data up to 42 eV, good fits are also obtained for Auger widths ranging from 30 to 70 meV, resulting in an uncertainty in the fit threshold position. We deduced from multiple fits, using various Auger widths in the aforementioned range, that the $4p_{3/2}$ threshold is between 40.10 and 40.27 eV. (We note that these Auger widths may be somewhat smaller than expected, but still reasonable given $4p$ decay widths measured in Xe, which are as small as 150 meV [52]). It is of interest to note that this also demonstrates a means of determining rough experimental values of the Auger decay widths of core-excited neutral atomic states.

An additional small feature can be noticed about 2 eV above the $4p$ threshold in both the Ru^+ and Ru^{2+} spectra, where there appears to be a new channel opening at $\sim$42.2 eV. We believe this feature is likely due to the $p_{1/2}$ fine-structure threshold. In solid Ru, the $p_{1/2}$ threshold is expected to be about 3 eV

above the $p_{3/2}$ [47], but may be lower in the atomic negative ion. However, a cusp associated with $5s \rightarrow 5p$ discrete excitations produced by inelastic $4p$ photoelectron scattering could potentially also explain this feature. Such a feature is seen, for example, in the partial $3p \rightarrow \varepsilon d$ photodetachment of Cr^- [16], when the dynamic polarization interaction for an outgoing electron is included in the theoretical calculations. If we assume a similar excitation energy for the scattering process (i.e., excitation from the $4p \rightarrow 4d$ core-excited neutral atomic state) as the first $5s \rightarrow 5p$ excitation ($4d^7 5p\,^5D_4$) from the ground state of Ru (3.262 375 eV [46]), the cusp should appear at ~43.4 eV. This is larger than the data suggest, but the currently very poor knowledge of the relevant core-excited Ru states does not allow us to exclude this possibility.

IV. SUMMARY AND CONCLUSIONS

We have reported absolutely scaled inner-shell photodetachment cross-section measurements for the Ru^- negative ion near and above the $4p$ excitation region in the photon energy range 29 to 91 eV. The absolute photodetachment cross sections for Ru^- leading to Ru^+, Ru^{2+}, and Ru^{3+} were measured at three photon energies, providing reference data for astrophysics. From measurements with high statistical precision near the $4p$ detachment onset, a best estimate for the $4p_{3/2}$ detachment threshold is determined to be between 40.10 and 40.27 eV, assuming an estimated Auger decay width of 30 to 70 meV. A direct two-electron detachment process, likely to Ru^+ $4p^5 4d^6 5s^2$, is observed in the Ru^{2+} spectrum, locating this state near 49 eV. Ru^{3+} is also observed, most likely originating from direct three-electron photodetachment to an autodetaching Ru^{2+} state near the Ru^{3+} ground state.

There is evidence that the existence of vacant states in the $4d$ inner shell of the Ru^- negative ion causes resonance interference effects between $4p$ electrons to the quasibound $4p^5 4d^8 5s^2$ excitations and the $4d \rightarrow \varepsilon f$ continuum, resulting in a net dip in the Ru^+ cross section (and the total calculated cross section) just below the $4p$ threshold and an enhancement just above the threshold. The interpretation is supported by theoretical calculations. The calculations reproduce most of the major observed features fairly well, although it would appear that there are additional autodetaching Ru excited states which carry some of the $4p \rightarrow 4d$ excitation cross section to Ru^+ that are missed in the sum. There remains, however, some structure not well described by the calculations, which suggests not all important channels or processes have been accounted for. The role of many-particle effects, intershell interaction, and polarization seems much more significant in Ru^- than in Fe^- photodetachment, as might be expected given the additional complexity of the heavier Ru^- ion. A more complete understanding of Ru^- photodetachment will have to await more elaborate theoretical calculations.

ACKNOWLEDGMENTS

This work was supported by US Department of Energy, Office of Science, Basic Energy Sciences, Chemical, Geoscience, and Biological Divisions. The ALS is funded by the DoE, Scientific User Facilities Division. N. D. Gibson and C. W. Walter acknowledge support from NSF Grants No. 0456916 and No. 0757976.

[1] X. Y. Xu, J. Z. Tang, W. Huang, W. Z. Zhao, and D. Y. Chen, J. Phys. B **23**, 3315 (1990).
[2] M. Martins, K. Goldenhusen, T. Richter, P. Wernet, and P. Zimmermann, J. Phys. B **39**, R79 (2006).
[3] S. B. Whitfield, R. Wehlitz, and M. Martins, Radiat. Phys. Chem. **70**, 3 (2004); B. Sonntag and P. Zimmermann, Rep. Prog. Phys. **55**, 911 (1992).
[4] J. C. Green, Acc. Chem. Res. **27**, 131 (1994).
[5] G. I. Bekov, V. S. Letokhov, and V. N. Radaev, J. Opt. Soc. Am. B **2**, 1554 (1985).
[6] G. Sprintschink, H. Sprintschink, P. Kirsch, and D. G. Whitten, J. Am. Chem. Soc. **98**, 2337 (1976).
[7] In *CRC Handbook of Chemistry and Physics*, edited by D. R. Lide (CRC Press, Boca Raton, FL, 2008), 89th ed.
[8] S. Salih and J. E. Lawler, J. Opt. Soc. Am. B **2**, 422 (1985).
[9] C. I. Callender, P. A. Hackett, and D. M. Rayner, J. Opt. Soc. Am. B **5**, 614 (1988).
[10] J.-J. Yeh and I. Lindau, At. Data Nucl. Data Tables **32**, 1 (1985); J.-J. Yeh, *Atomic Calculations of Photoionization Cross Sections and Asymmetry Parameters* (Gordon and Breach, Langhorne, PA, 1993).
[11] R. Gotter, W.-K. Siu, R. A. Bartynski, S. L. Hulbert, X. Wu, M. Zitnik, and H. Nozoye, Phys. Rev. B **61**, 4373 (2000).
[12] R. Gotter, R. A. Bartynski, S. L. Hulbert, X. Wu, H. Nozoye, and M. Zitnik, J. Electron Spectrosc. Relat. Phenom. **93**, 201 (1993).
[13] A. de Siervo, R. Landers, G. G. Klein, S. G. C. De Castro, and J. Morais, J. Electron Spectrosc. Relat. Phenom. **101-103**, 751 (1999).
[14] W. Drube, R. Treusch, R. Dahn, M. Griebenow, M. Grehk, and G. Materlik, J. Electron Spectrosc. Relat. Phenom. **79**, 223 (1996).
[15] P. L. Norquist, D. R. Beck, R. C. Bilodeau, M. Scheer, R. A. Srawley, and H. K. Haugen, Phys. Rev. A **59**, 1896 (1999).
[16] V. K. Ivanov, L. P. Krukovskaya, and G. Yu Kashenock, J. Phys. B **31**, 239 (1998).
[17] A. M. Covington *et al.*, Phys. Rev. A **66**, 062710 (2002).
[18] R. C. Bilodeau, I. Dumitriu, N. D. Gibson, C. W. Walter, and N. Berrah, Phys. Rev. A **80**, 031403 (2009).
[19] I. Dumitriu, R. C. Bilodeau, T. W. Gorczyca, C. W. Walter, N. D. Gibson, A. Aguilar, Z. D. Pesić, D. Rolles, and N. Berrah, Phys. Rev. A **81**, 053404 (2010).
[20] R. C. Bilodeau, J. D. Bozek, N. D. Gibson, C. W. Walter, G. D. Ackerman, I. Dumitriu, and N. Berrah, Phys. Rev. Lett. **95**, 083001 (2005).
[21] R. C. Bilodeau, N. D. Gibson, J. D. Bozek, C. W. Walter, G. D. Ackerman, P. Andersson, J. G. Heredia, M. Perri, and N. Berrah, Phys. Rev. A **72**, 050701(R) (2005).
[22] N. Berrah, R. C. Bilodeau, I. Dumitriu, J. D. Bozek, N. D. Gibson, C. W. Walter, G. D. Ackerman, O. Zatsarinny, and T. W. Gorczyca, Phys. Rev. A **76**, 032713 (2007).

[23] R. Middleton, *A Negative Ion Cookbook* (Department of Physics, University of Pennsylvania, Philadelphia, PA, 1990).
[24] A. G. Shenstone and W. F. Meggers, J. Res. Natl. Bur. Stand. (US) **61**, 373 (1958).
[25] T. A. Carlson, C. W. Nestor Jr., N. Wasserman, and J. D. McDowell, At. Data **2**, 63 (1970).
[26] E. M. Gullikson, R. Korde, L. R. Canfield, and R. E. Vest, J. Electron Spectrosc. Relat. Phenom. **80**, 313 (1996).
[27] R. P. Madden, D. L. Ederer, and K. Codling, Phys. Rev. **177**, 136 (1969).
[28] K. Schulz, M. Domke, R. Püttner, A. Gutiérrez, G. Kaindl, G. Miecznik, and C. H. Greene, Phys. Rev. A **54**, 3095 (1996).
[29] G. C. King, M. Tronc, F. H. Read, and R. C. Bradford, J. Phys. B **10**, 2479 (1977).
[30] Based on similar experiments detecting these charged states: R. A. Phaneuf (private communication).
[31] [http://www.sisweb.com/simion.htm].
[32] J. C. Fuggle and N. Mårtensson, J. Electron Spectrosc. Relat. Phenom. **21**, 275 (1980).
[33] H. Kjeldsen, P. Andersen, F. Folkmann, B. Kristensen, and T. J. Andersen, J. Phys. B **34**, L353 (2001).
[34] N. Berrah *et al.*, Phys. Rev. Lett. **87**, 253002 (2001).
[35] H.-L. Zhou, S. T. Manson, L. Vo Ky, N. Feautrier, and A. Hibbert, Phys. Rev. Lett. **87**, 023001 (2001).
[36] T. W. Gorczyca, O. Zatsarinny, H.-L. Zhou, S. T. Manson, Z. Felfli, and A. Z. Msezane, Phys. Rev. A **68**, 050703(R) (2003).
[37] T. W. Gorczyca, Radiat. Phys. Chem. **70**, 407 (2004).
[38] N. Berrah, R. C. Bilodeau, G. D. Ackerman, J. D. Bozek, G. Turri, E. Kukk, W. T. Cheng, and G. Snell, Radiat. Phys. Chem. **70**, 491 (2004).
[39] C. W. Walter, N. D. Gibson, R. C. Bilodeau, N. Berrah, J. D. Bozek, G. D. Ackerman, and A. Aguilar, Phys. Rev. A **73**, 062702 (2006).
[40] N. D. Gibson, C. W. Walter, O. Zatsarinny, T. W. Gorczyca, G. D. Akerman, J. D. Bozek, M. Martins, B. M. McLaughlin, and N. Berrah, Phys. Rev. A **67**, 030703(R) (2003).
[41] G. Y. Kashenock and V. K. Ivanov, J. Phys. B **39**, 1379 (2006).
[42] J. R. Peterson, Y. K. Bae, and D. L. Huestis, Phys. Rev. Lett. **55**, 692 (1985).
[43] Y. K. Bae and J. R. Peterson, Phys. Rev. A **32**, 1917 (1985).
[44] H. Kjeldsen, J. Phys. B **39**, R325 (2006).
[45] P. G. Burke and K. A. Berrington, *R-Matrix Theory of Atomic and Molecular Process* (IOP Publishing, Oxford, 1993); K. A. Berrington, W. B. Eissner, and P. N. Norrington, Comput. Phys. Commun. **92** (1995).
[46] NIST Atomic Spectra Database online: [http://physics.nist.gov/asd3].
[47] M. Cardona and L. Ley (editors), *Photoemission in Solids I: General Principles* (Springer-Verlag, Berlin, 1978).
[48] G. H. Wannier, Phys. Rev. **90**, 817 (1953).
[49] P. N. Juranic and R. Wehlitz, Phys. Rev. A **78**, 033401 (2008); A. Emmanouilidou, *ibid.* **76**, 054701 (2007); J. B. Bluett, D. Lukic, and R. Wehlitz, *ibid.* **69**, 042717 (2004).
[50] E. P. Wigner, Phys. Rev. **73**, 1002 (1948).
[51] T. Andersen, Phys. Rep. **394**, 157 (2004); D. J. Pegg, Nucl. Instrum. Methods B. **261**, 138 (2007); M. Ya Amusia, G. F. Gribakin, V. K. Ivanov, and L. V. Chernysheva, J. Phys. B **23**, 385 (1990).
[52] S. Heinäsmäki, H. Aksela, J. Nikkinen, E. Kukka, A. Kivimäki, S. Aksela, and S. Fritzsche, J. Electron Spectrosc. Relat. Phenom. **137-140**, 281 (2004).